An ADTS Toolbox for Automatically Interpreting Active Distributed Temperature Sensing Measurements

Nataline Simon, Olivier Bour

Groundwater

Methods Note/

An ADTS Toolbox for Automatically Interpreting Active Distributed Temperature Sensing Measurements

by Nataline Simon[1] and Olivier Bour[2]

Abstract

Active distributed temperature sensing (ADTS) experiments are very useful to provide in-situ and distributed estimates of thermal conductivities of the subsurface and of groundwater flows. However, the data interpretation can be seen as difficult considering the large amount of data collected along a heated fiber-optic cable and the lack of associated tools for their automated analysis. In this context, we developed an automated routine program for the interpretation of ADTS measurements: the ADTS Toolbox. It contains several codes written in MATLAB that calculate, for each measurement point located along a heated section, both the thermal conductivity of the surrounding material and the groundwater flux. In addition, it provides uncertainties on the estimated thermal conductivities and fluxes according to the temperature resolution (noise) or to errors on temperature measurements. By offering the possibility of automatically interpreting ADTS measurements, the ADTS Toolbox facilitates the use and interpretation of ADTS experiments for characterizing at high resolution the groundwater flows distribution and for imaging the thermal conductivities variability.

Introduction

Heat has been widely used as a tracer over the past 80 years (Anderson 2005; Kurylyk et al. 2019) and so much more since the development of distributed temperature sensing (DTS) in hydrologic sciences (Selker et al. 2006; Tyler et al. 2009). DTS technology provides continuous temperature records through space and time along fiber optic (FO) cables at high spatial and temporal resolutions. Among DTS applications, active methods (ADTS) have been recently developed, opening new promising perspectives for subsurface characterization in many applications (Bense et al. 2016). It mainly consists in continuously monitoring the temperature changes induced by a heat source along a FO cable. When applied in the subsurface, the difference of temperature measured between a heated and a non-heated FO cable depends on both the thermal conductivity of the media surrounding the cable and the groundwater flow occurring in boreholes or in sediments (Read et al. 2014; Bakker et al. 2015; Simon et al. 2021).

ADTS methods have already been used for different applications, especially for characterizing borehole flows or groundwater fluxes in fractured media or sedimentary aquifers in various conditions, like in open boreholes (Leaf et al. 2012; Liu et al. 2013; Banks et al. 2014; Read et al. 2014; Hausner et al. 2015; Read et al. 2015), in sealed boreholes (Coleman et al. 2015; Klepikova et al. 2018; Selker and Selker 2018; Maldaner et al. 2019; Munn et al. 2020), or else in direct contact within sedimentary aquifers (Bakker et al. 2015; Des Tombe et al. 2019; del Val et al. 2021). It has also been used for dam and dike monitoring to detect seepage flows (Perzlmaier et al. 2004; Aufleger et al. 2007; Su et al. 2017;

[1]Corresponding author: University of Rennes, CNRS, Géosciences Rennes, UMR 6118, 35000 Rennes, France; nataline.simon2@gmail.com

[2]University of Rennes, CNRS, Géosciences Rennes, UMR 6118, 35000, Rennes, France

Ghafoori et al. 2020) or for geothermal applications to infer the thermal conductivities distribution along boreholes (Galgaro et al. 2018; Vélez Márquez et al. 2018; Zhang et al. 2020).

Following the first applications and developments, which clearly showed a correlation between the flow and the temperature elevation measured during heat injection (Perzlmaier et al. 2004; Read et al. 2014; Sayde et al. 2015), we recently proposed and validated a general framework for interpreting ADTS measurements conducted in saturated porous media (Simon et al. 2021). We showed that the distribution of thermal conductivities and groundwater fluxes can be both estimated by analyzing and modeling each thermal response curve obtained along the heated section, demonstrating the potential of ADTS experiments to characterize the spatial distribution of hydraulic and thermal properties in the subsurface.

However, the method proposed by Simon et al. (2021) relies on a manual interpretation of each thermal response curve recorded along the heated section, which limits its application. Considering the large amount of data collected and the lack of associated tools for their automated analysis and interpretation, we propose here the ADTS Toolbox which is an automated routine that allows interpreting ADTS measurements achieved in the subsurface. By interpreting ADTS experiments, this toolbox is complementary to the one proposed in the past for interpreting temperature profiles (Voytek et al. 2014; Kurylyk and Irvine 2019) or else for visualizing DTS data (Domanski et al. 2020).

In the following, we first present the theoretical background used to interpret ADTS measurements before introducing the ADTS Toolbox, which contains the different codes written in MATLAB that automatically calculate, for each measurement point located along a heated section, both the thermal conductivity of the surrounding material and the groundwater flux. It also provides uncertainties on the estimated thermal conductivities and fluxes according to the temperature resolution (noise) or to errors on temperature measurements. In the Results section, an example of application of the ADTS Toolbox to interpret field data is proposed.

Theoretical Background

The automated approach developed to interpret ADTS measurements is based on the work of Simon et al. (2021), who proposed and experimentally validated two interpretation methods to analyze the temperature increase measured during ADTS experiments conducted using a single heated FO cable. In this configuration, the FO cable is electrically heated through its steel armoring and the elevation in temperature continuously monitored all along the heated section. It means that a single FO cable is used as a heat source and as a measurement tool to monitor the surrounding temperature (Read et al. 2014; Bense et al. 2016; Selker and Selker 2018; Bakx et al. 2019; Simon et al. 2021). The groundwater fluxes are assumed to be perpendicular to the heated FO cable.
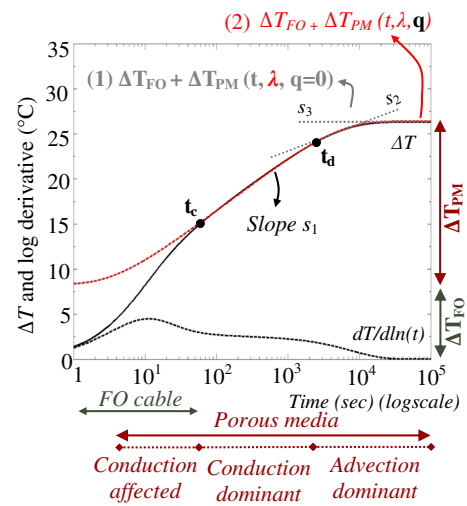

Figure 1. Principle of the interpretation of thermal response curves (represented by the black line) collected during ADTS measurements (following Simon et al. 2021). The black dotted line corresponds to the log-derivative of temperature. First, the temperature rise ΔT_{PM} during the conduction-dominant period, for $t_c < t < t_d$, can be reproduced using the Moving Instantaneous Line Source (MILS) model considering $q = 0$ m/s (gray line). Then, ΔT_{PM} during both conduction-dominant and the advection-dominant periods can be reproduced using the MILS model considering the groundwater flow (red line).

The general approach proposed in Simon et al. (2021) is based on the interpretation of the typical thermal response curve (Figure 1) expected during the heating periods. Figure 1 shows the evolution of the temperature ΔT through time measured at a specific location along the heated cable over the heating period (black line) and its log-derivative (black dotted line), both represented in a semi-log graph.

At early times, the measured temperature increase ΔT depends on the thermal properties of the FO cable (ΔT_{FO}) and the heat produced is stored within the FO cable inducing a large temperature increase (del Val et al. 2021; Simon et al. 2021). As soon as the heat reaches the material surrounding the FO cable, conduction starts controlling heat transfers in the porous media. Thus, during the conduction-affected period, the evolution of the temperature is simultaneously controlled by heat storage in the cable as well as heat transfer occurring in the porous medium. Then, for $t > t_c$, the temperature evolution is no longer sensitive to the effect of the heated FO cable. At this point, temperature rise becomes exclusively controlled by heat conduction and advection occurring in the porous media. The associated temperature elevation (ΔT_{PM}) can be then separated in two different stages. First, the conduction-dominant period occurs from $t = t_c$ up to $t = t_d$. During this stage, a gradual increase of temperature is observed (Figure 1) and the temperature rise is independent of the flow and exclusively controlled by the thermal conductivity of the porous media surrounding the cable. When $t > t_d$, the temperature rise departs from the conduction regime and a decreasing rate of temperature

rise marks the start of the advection-dominant stage. By dissipating the heat produced, heat advection limits the temperature rise leading to the progressive stabilization of temperature for late times (Diao et al. 2004). After a transition period, which can be approximated by a slope s_2, the temperature stabilizes at the maximum ΔT (straight line with null slope s_3) meaning that the additional heat injected is fully dissipated by advection (steady-state conditions). The intensity of the flow controls the temperature increase and stabilization. Thus, for a given value of thermal conductivity, higher values of ΔT can be associated with lower fluxes. Full details about the interpretation of the temperature rise associated to ADTS experiments are given in Simon et al. (2021).

The analytical approach proposed and validated by Simon et al. (2021) focuses on the interpretation of the second part of the thermal response curve (ΔT_{PM}). Since ΔT_{FO} is constant for $t > t_c$, being only dependent on the heat injected and on the properties of the FO cable, its value can be graphically estimated and fixed before interpreting the evolution of ΔT_{PM}. Once ΔT_{FO} is estimated, the evolution of ΔT_{PM} over time can be modeled using the Moving Instantaneous Line Source (MILS) model (Carslaw and Jaeger 1959; Zubair and Chaudhry 1996; Sutton et al. 2003). By considering an initial thermal equilibrium T_0, the thermal response ΔT_{PM} ($\Delta T = T - T_0$) along the line source is given in x-y direction by:

$$\Delta T_{\mathrm{PM}}(x, y) = \frac{Q}{4\pi\,\lambda}\,\exp\left[\frac{q\,x}{2D_t}\,\frac{\rho_w c_w}{\rho c}\right]$$
$$\int_{\frac{x^2+y^2}{4tD_t}}^{\infty} \exp\left[-\Psi - \left(\frac{x^2+y^2}{D_t}\right)\frac{q^2}{16D_t\Psi}\,\frac{\rho_{w^2}c_{w^2}}{\rho^2 c^2}\right]\frac{d\Psi}{\Psi}$$

(1)

With q the groundwater flux in x-direction (or specific discharge) (m/s) at a given location and Q the constant and uniform heating rate power (W/m). The coordinates x and y correspond to the distance from the heat source, located at $x = 0$ and $y = 0$. ρc is the volumetric heat capacity of the rock-fluid matrix (J/m^3/K) and $\rho_w c_w$ the volumetric heat capacity of water (J/m^3/K). D_t is the thermal diffusivity coefficient (m^2/s) and the ratio between λ, the bulk thermal conductivity (W/m/K), and ρc. Ψ is a change of variable.

As shown in Figure 1, Equation (1) is firstly used to model the temperature rise for $t_c < t < t_d$, during the conduction-dominant period assuming $q = 0\,\mathrm{m/s}$ (gray line), to deduce thermal conductivity of the material surrounding the heating FO cable. Then, Equation (1) is used during both conduction-dominant and the advection-dominant periods for estimating groundwater flow (red line). This step-by-step procedure is used in the following for estimating the distribution of thermal conductivities and groundwater fluxes through the ADTS Toolbox.

Using the ADTS Toolbox

The ADTS Toolbox offers the possibility of automatically interpreting each thermal response curve collected all along the heated section. For that, an interpretation routine, based on the interpretation methods proposed by Simon et al. (2021), is applied and repeated for each measurement point providing distributed estimates of both the thermal conductivities and the fluxes. The ADTS Toolbox contains several MATLAB codes on which the data interpretation relies. The user guide included in the ADTS Toolbox details the preparation of experimental data and step-by-step instructions on the use of each MATLAB code and on the integration of the data inputted into them. Figure 2 presents the different steps and associated MATLAB codes proposed to interpret ADTS measurements using the ADTS Toolbox. The data analysis includes a preliminary preparation step and the automated data interpretation, divided in two steps: (1) the estimation of the thermal conductivities; (2) the estimation of the fluxes.

Preliminary Preparation Step

Before the automated interpretation steps, a preliminary preparation step is required as detailed in Figure 2. Then, two prerequisite parameters used for the data interpretation, ΔT_{FO} and the reference period, have to be manually set.

First, theoretically, the interpretation methods would require delimiting the conduction-dominant period for each thermal response curve (Simon et al. 2021). As shown in Figure 1, this stage can easily and graphically be defined since the associated temperature evolution trends as a straight line from $t = t_c$ up to $t = t_d$ in a semi-log representation (slope s_1). Note that the time t_c is also marked by the end of the hump made by the log-time derivative of temperature. However, the duration of the conduction-dominant period varies from one measurement point to another according to the flow intensity and the automated delimitation of the conduction-dominant period for each thermal response curve is not possible, especially because of the temperature resolution. Thus, the user has to manually define a reference period over which the conduction-dominant stage is observed for any thermal response curve. In practice, this reference period can be defined using the thermal response curve showing the shortest conduction-dominant period, which is generally associated to the smallest value of ΔT measured at the end of the experiment.

Then, the automated data interpretation requires defining the value of ΔT_{FO}, which is constant for $t > t_c$ and independent of both the thermal properties of the material and the flow conditions. Ideally, it should be estimated through laboratory tests or using numerical models (Simon et al. 2021). However, it can also be graphically estimated for a single point measurement and extrapolated to all other data points since it depends only on the properties of the FO cable and on the constant and uniform heating rate power. For that, the user is encouraged using the MATLAB code *Interpretation_single_thermal_reponse_curve.m*. The principle consists in manually interpreting a single thermal response curve by fitting the temperature rise with the MILS model for $t > t_c$, in order to calibrate and deduce the value of ΔT_{FO}.
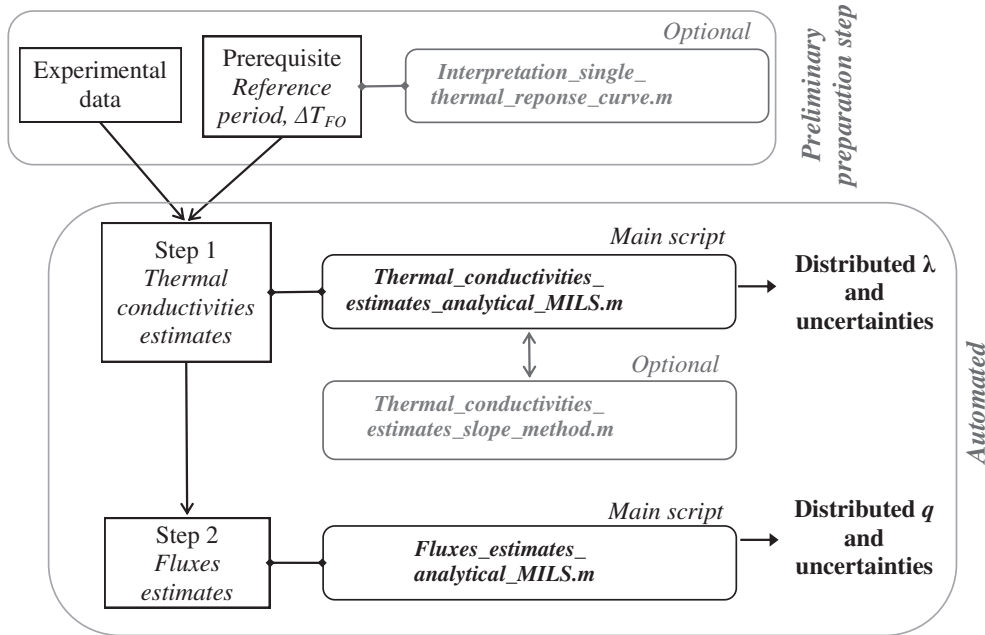
Figure 2. Description of the different steps of the ADTS measurements interpretation using the ADTS Toolbox.

Step 1: Estimating Thermal Conductivities

The first step of the automated data interpretation aims to estimate the thermal conductivities all along the heated section, as well as the associated uncertainties (Figure 2). First, an analytical approach is proposed in the MATLAB code called *Thermal_ conductivities_estimates_analytical_MILS.m*. The user defines a consistent range of values of thermal conductivities that should be tested in accordance with the material where the ADTS measurements were conducted. For each value of thermal conductivity tested, the MILS model is used considering $q = 0$ m/s to model the temperature increase ΔT_{PM}, at which the value of ΔT_{FO} is added to model a theoretical thermal response curve. Then, for each measurement point, the RMSE (root-mean-square error) between each predicted model and the measured temperature during the reference period is calculated. The lowest RMSE obtained between the data and the model for each measurement point allows defining the optimal value of the thermal conductivity. The MATLAB code was written to apply and repeat the principle described above for each measurement point providing distributed estimates of the thermal conductivities.

To go further, the program also automatically estimates the uncertainties on thermal conductivities associated to the temperature resolution or to the uncertainty of the estimated temperature, which can be evaluated following the method proposed by Des Tombe et al. (2020). To compute these uncertainties, Equation (1) is used to model the temperature increase expected after a given heating duration according to the value of thermal conductivity and for $q = 0$ m/s. It provides the theoretical curve $\Delta T = f (\lambda, q = 0)$, which allows associating a value of ΔT to a value of thermal conductivity, used to estimate the error on thermal conductivity related to

the temperature resolution. Since a negative relationship exists between ΔT and λ (Simon et al. 2021), a temperature increase of $\Delta T + X \,^{\circ}\text{C}$ is associated to a value of thermal conductivity of $\lambda = \lambda_{min}$ and a temperature increase of $\Delta T - X \,^{\circ}\text{C}$ is associated to a value of thermal conductivity of $\lambda = \lambda_{max}$. Thus, the value of thermal conductivity is estimated for each measurement point between λ_{min} and λ_{max}, according to the temperature resolution.

Once calculations are done, the resulting plots, automatically generated, show (1) the distributed estimated values of thermal conductivities and associated uncertainties; (2) a comparison between an experimental curve, chosen by the user or set by default, and the associated modeled curve; and (3) the effect of the temperature resolution on the thermal conductivity estimate, by plotting the modeled temperature increases associated to λ_{min} and λ_{max}.

This analytical approach is efficient and reliable to estimate the thermal conductivities. However, it requires defining the value of ΔT_{FO} of which the results of thermal conductivities estimates are highly sensitive. Thus, in complement, we introduce the MATLAB code *Thermal_conductivities_estimates_slope_method.m* (see Figure 2) that relies on a graphical approach to estimate thermal conductivities. For each measurement point, the code calculates the value of the slope s_1 that is the temperature increase observed during the reference period using the *polyfit* and *polyval* functions available in MATLAB. Once the slope is calculated, the value of the thermal conductivity is simply deduced from $\lambda = Q/4\pi s_1$ (Simon et al. 2021). The principle is then repeated for each measurement point. This approach is less accurate than the analytical one since the calculation of the slope highly depends on temperature resolution, especially when the conduction-dominant stage is short (typically when it is

less than half an order of magnitude). However, the main advantage of the graphical method is that the interpretation is independent of the value of ΔT_{FO}. As a reminder, this step is optional, since thermal conductivities can be estimated using the analytical approach. Nevertheless, it can help strengthening the estimates. Once calculations are done, the result plot allows comparing the distributed values of thermal conductivities estimated with the analytical approach and the one estimated with the graphical approach. If the estimated thermal conductivities are similar using both approaches, the value of ΔT_{FO} can be validated. If not, the user should reconsider the value of ΔT_{FO} before rerunning the code *Thermal_conductivities_estimates_analytical_MILS.m*. Since the fluxes are estimated in the next step using the values of thermal conductivities defined with the latter code, a good adjustment of ΔT_{FO} is essential to ensure a good estimate of fluxes.

Step 2: Estimating Fluxes

The MATLAB code *Fluxes_estimates_analytical_MILS.m* permits to automatically estimate the fluxes all along the heated section, as well as their associated uncertainties (Figure 2). Once the value of the thermal conductivity is defined, the MILS model can be used to reproduce the temperature increase observed for any $t > t_c$ (red line in Figure 1). Thus, the analytical solution is used to model the temperature increase by varying the value of the groundwater flux over a consistent range defined by the user. For each measurement point, the RMSE is calculated between the model and the measured temperature during both the conduction- and the advection-dominant periods. The optimal value of the flux is defined from the lowest value of RMSE. The repetition of this routine for each measurement point allows estimating the fluxes distribution.

The uncertainties on fluxes estimates associated to a given error on temperature measurement or due to the estimated temperature resolution are also automatically calculated, with the same principle as the one used in step 1 for thermal conductivities uncertainties. Since a negative relationship exists between ΔT and q, a temperature increase of $\Delta T + X\,^\circ C$ is associated to a value of thermal conductivity of $q = q_{min}$ and a temperature increase of $\Delta T - X\,^\circ C$ is associated to a value of thermal conductivity of $q = q_{max}$. Thus, the value of groundwater flux is estimated for each measurement point between q_{min} and q_{max}, according to the temperature resolution.

For this step, the input parameters, which are identical to the one used while estimating the thermal conductivities, are automatically loaded. Once the calculations are achieved, the result plots are automatically generated and show (1) the distributed estimated values of fluxes and associated uncertainties along the heated section; (2) a comparison between an experimental curve, chosen by the user or set by default, and a modeled one; and (3) the effect of the temperature resolution on the flux estimate, by plotting the modeled temperature increases associated

to both values q_{min} and q_{max}. The latter plot allows visually comparing the model and the experimental data.

Note that the advection-dominant stage may not be reached at the end of the heating period either because there is no flow at the point of measurement or because the heating duration has not been long enough to observe this stage, especially for very low fluxes that require days or weeks to be investigated (Simon et al. 2021). Such cases are automatically identified by the code. The MILS model is used to model the temperature increase expected at the end of the heating period under no flow-condition according to the value of the thermal conductivity. If this value is similar to the measured temperature (also recorded at the end of the heating period), it means that the advection-dominant stage is not reached at the end of the heating period. Thus, an estimate of the minimum flux value q_{lim} can be calculated. It corresponds to the value of the flux below which the measured temperature increase would be identical whatever the value of flux considered. In other words, although the flux cannot be determined precisely, its upper limit q_{lim}, can be assessed.

Validation

The method of automation developed here was tested on different datasets in different environments, including numerical simulations and experimental thermal responses measured in perfectly-controlled conditions presented in Simon et al. (2021). The toolbox estimated thermal conductivities and fluxes are in very good agreement with the expectations with less than 3% of error. The error mainly depends on the definition of ΔT_{FO} and of the reference period.

Example

We demonstrate the ADTS Toolbox for an experimental dataset collected in a streambed. A file including the data set, the filled-out MATLAB scripts, the results, and the associated plots are provided to the users as an example of application.

Data Acquisition

The experiment was conducted on the experimental site of Signy located in the Sélune catchment, in western France (Fovet et al. 2020). At this location, pumping wells located near the Sélune river floodplain induce a permanent infiltration of the river water into the aquifer. In this context, the aim of the experiment was to quantify the spatial variability of the river water infiltration. The setup consisted in longitudinally deploying a heatable FO cable into the streambed sediments of the river. The cable was buried at approximately 8-cm depth using a plow which limits the alteration of the riverbed and allows for a good control of the burial depth. The FO cable is a 3.8-mm-diameter cable containing 4 multimode 50/125-µm fibers (BruSens cable; reference LLK-BSTE 85 °C). The temperature evolution was measured every 12.5 cm at a 20 s sampling interval using a Silixa Ultima S DTS unit set up in double-ended configuration (van de

Giesen et al. 2012). The effective spatial resolution of the unit was estimated between 51 and 67 cm following the methodology proposed in Simon et al. (2020). The DTS unit was calibrated using two calibration baths (a warm one and a cold one) and the accuracy and precision of the acquired data were verified using PT100 (0.1 °C) and RBR SoloT (0.002 °C accuracy) probes. The relative uncertainty of temperature measurements was estimated to 0.03 °C and the absolute one at 0.15 °C. The heat experiment was conducted by continuously injecting electricity, for almost 4 h, in a 40 m-section of cable using a Silixa Heat Pulse Control System, providing a power intensity of 30.13 W/m along the cable. A figure presenting the experimental setup is provided as supplement in the user guide.

Use of the ADTS Toolbox

The data were interpreted following the different steps described in Figure 2, starting with the preliminary step. For the smallest values of ΔT measured at the end of the experiment, the conduction-dominant period was graphically delimitated between $t \approx 90$ s and $t \approx 27$ min. Thus, the reference period was set over the heating duration between 251 s and 27 min. Note that even if the conduction-dominant period actually starts earlier, selecting a later point as start of the reference period can prevent the potential effect of the temperature resolution on data interpretation. The value of ΔT_{FO}, which depends on both the FO cable and the heating rate power, was fixed at 12.11 °C using the MATLAB code *Interpretation_single_thermal_reponse_curve.m*. This result is in very good agreement with previous numerical and experimental results using the same FO cable (Simon et al. 2021).

Then, the script *Thermal_conductivities_estimates_analytical_MILS.m* was used to estimate the value of the thermal conductivity and its associated uncertainty for each measurement point. The range of thermal conductivities tested was fixed from 0.8 to 5 W/m/K with a step of 0.01 W/m/K in accordance with the sediments observed

in the streambed, that is, saturated clay, sand, and gravels (Stauffer et al. 2013). In complement, the script *Thermal_conductivities_estimates_slope_method.m* was used to estimate the thermal conductivities and to validate the value of ΔT_{FO}. Then, the script *Fluxes_estimates_analytical_MILS.m* was used to estimate the value of the flux and its associated uncertainty for each measurement point. In total, 100 values of fluxes, logarithmically distributed between 1×10^{-7} and 5×10^{-5} m/s, were tested to estimate the effective values of fluxes. For each of these steps, the value of the temperature resolution was set at 0.1 °C and the associated uncertainties on thermal conductivities and fluxes estimates were calculated.

Results

The distributions of thermal conductivities and fluxes, as well as their associated uncertainties, are displayed in Figure 3. The thermal conductivity of the sediments varies between 2.48 and 2.88 W/m/K (Figure 3a) with uncertainties ±0.03 W/m/K. The high resolution offers a precise description of the streambed properties. Note that the consistency of these estimates was verified using the graphical approach which validates the estimated value of ΔT_{FO}. Detailed results are not presented here but included as supplement in the toolbox.

The vertical fluxes (losing stream) vary between 2.17×10^{-6} and 1.67×10^{-5} m/s (0.18–0.39 m/d), over more than an order of magnitude (Figure 3b). The approach highlights the spatial variability of fluxes which could not be characterized at such high resolution with any other method. Results show that the uncertainty on flow estimate depends on the value of the flow. As observed between 105.5 and 112 m, the uncertainty is proportionally higher for low fluxes, the method being less resolving. Results also show that for some spots, marked by blue points in Figure 3b, flow cannot be estimated from data collected, since no departure from conduction-dominant stage is observed at the end of the
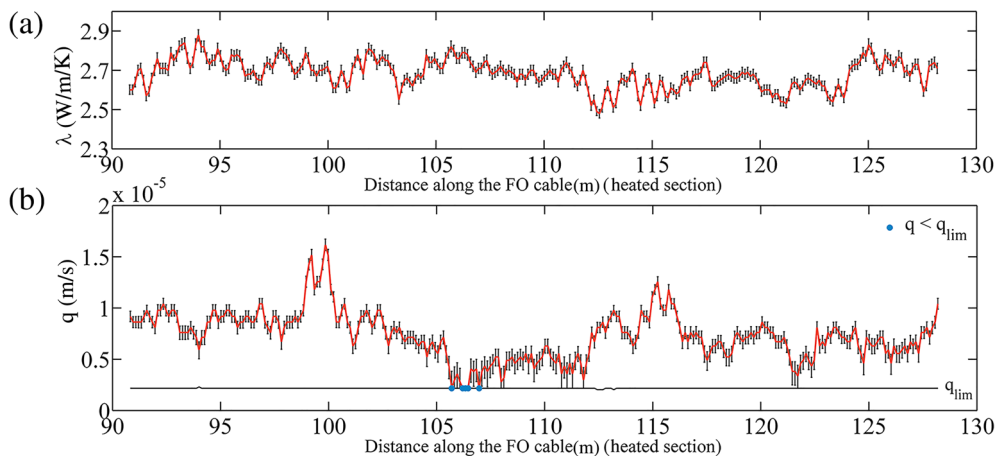

Figure 3. (a) Estimated thermal conductivities and associated uncertainties all along the heated section. (b) Estimated fluxes and associated uncertainties all along the heated section. The blue points correspond to spots where the low values of q cannot be estimated and are only defined as $q < q_{lim}$.
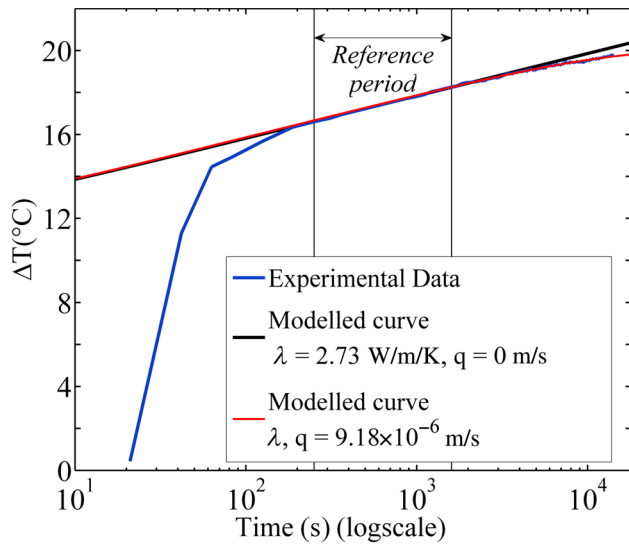
Figure 4. Example of results obtained using the ADTS Toolbox for $d = 101.5$ m (blue curve). The temperature rise is reproduced for $t > 269$ s using the MILS model (red curve) by considering a thermal conductivity $\lambda = 2.73$ W/m/K and a groundwater flux $q = 9.18 \times 10^{-6}$ m/s.

experiment, meaning that advection is not reached at the end of the experiment for these data points. Note that the heating duration for this experiment is relatively short (4 h) limiting the determination of low groundwater fluxes (Simon et al. 2021).

Using the estimated thermal conductivities and the fluxes, the MATLAB codes model the temperature increase expected for each measurement point, as illustrated in Figure 4. The codes allow a very good reproduction of the measured temperature increase, with an RMSE between the model and the data being around 0.1 °C during the reference period and around 0.4 °C for the entire heating duration. The large amount of data considered in the second case tends to increase the value of the RMSE despite the good quality of the model.

Discussion

The automated approach developed here is based on the work of Simon et al. (2021) who largely discussed the limitations of the method, its applicability, ideal experimental conditions (choice of the FO cable, power supply, experimental setup, heating durations etc.), and uncertainties. These points are therefore not discussed here and following paragraphs focus on discussion points associated to the use of the ADTS Toolbox and not to the interpretation method.

Considering the large amount of data collected, the manual interpretation of ADTS measurements is impossible. In this context, the ADTS Toolbox appears as the first free tool available for automatically interpreting ADTS measurements. Thus, its use allows a considerable save of time. For the presented example (295 measurement points with 4 h of heating), the running time of the ADTS Toolbox is quite reasonable since around few hours were

required to interpret the data presented in the example using an Intel 2.60 GHz processor.

The automated interpretation of data is divided in two steps that are the estimation of thermal conductivities and the estimation of groundwater fluxes. This allows for a better adaptation to the user objectives. For instance, when no groundwater fluxes are expected, the users could exclusively focus on the first step on the automated data interpretation that provides thermal conductivities along the heated section. The second step would be achieved for any user who aims estimating groundwater fluxes and their distribution. However, this two-steps interpretation method can be limited when large values of groundwater fluxes occur. Indeed, for $q > 8 \times 10^{-5}$ m/s, the stabilization period (t_d) is reached in less than 60 s (Simon et al. 2021). In such cases, the temperature elevation does not show any conduction-dominant period making the definition of a reference period and therefore the estimation of the thermal conductivity impossible. However, it remains possible to estimate groundwater fluxes by setting an approximate value of λ before estimating q.

The developed tool can be directly used to interpret any ADTS measurements as soon as the experimental setup consists in a single heated FO cable deployed in a saturated porous media. Here, the field experiment was conducted with cables containing optical fibers surrounded by a steel core and a plastic jacket. The thermal and electrical properties of these simple cables are ideal to conduct ADTS experiments. Their thermal conductivity is high enough to ensure a fast and significant thermal response and their resistance (0.35 Ω/m) is high enough to easily inject a sufficient electrical power (at least 15 watts per meter of cable) which highly improves the resolution of measurements and decreases errors on flux estimates. Some other authors propose to conduct ADTS experiments with hydride or composite FO cables, including optical fiber and copper wires in a single cable (among others, Coleman et al. 2015; Maldaner et al. 2019; Munn et al. 2020; Hakala et al. 2022). Although their low resistance generally limits the electrical power injected in the system, which decreases the resolution of measurements, such cables may present some other advantages, in particular to achieve experiments with a low voltage. In such case, the ADTS Toolbox remains fully adapted to interpret the data. The user should take into account the geometry of the cable to define the exact location of the copper wires and the optical fibers regarding to the flow direction, which can be an important uncertainty source. This may be done by adjusting the distance between the heat source and the FO cable.

Furthermore, the ADTS Toolbox can also be used when the setup consists in using a heating cable combined with a separate FO cable. However, once the cables are installed, it may be difficult to check if the two cables are sticked to each other and to define the exact location of the heating cable according to the flow direction (Des Tombe et al. 2019). Likewise, the temperature evolution can be simulated at any distance from the heat source,

when the heat source is far away from the FO cable. It allows modeling heat transport between boreholes for instance or for active heat tracer test conducted at large scale into unconsolidated sedimentary aquifers (Bakker et al. 2015). In both cases, the value of x is set as the distance between the heat source (line source) and the FO cable. Note that ΔT_{FO} should be set to 0 since only the temperature increase induced by the heat transport within the porous media is measured (ΔT_{PM}). However, heat dispersion could occur between the heat source and the FO cable (Des Tombe et al. 2019), meaning that the user may need to consider longitudinal and transversal dispersivities.

The ADTS Toolbox is best suited for ADTS measurements conducted in fully saturated porous media, as in Bakker et al. (2015), Des Tombe et al. (2019), and Simon et al. (2021). It cannot be used to interpret ADTS measurements collected in free water, for instance in open boreholes (Read et al. 2014). However, its use is appropriate in well environment as soon as the investigated borehole is sealed using packers, flexible borehole liners (Coleman et al. 2015) or temporary grout (Klepikova et al. 2018). The borehole can also be permanently sealed with grout once the FO cables are installed (Selker and Selker 2018; Zhang et al. 2020), but the DTS cables can also be installed behind the borehole casing, in contact with the aquifer materials (del Val et al. 2021). In such cases, the use of the ADTS Toolbox could require discarding the temperature increase induced by the grout and observed before heat reaches the sediments or materials surrounding the borehole (Zhang et al. 2020).

Conclusion

The ADTS Toolbox presented in this study offers the possibility to automatically interpret ADTS measurements (active distributed temperature sensing) collected in fully saturated porous media. Through some adjustments, the ADTS Toolbox can also be used to interpret data collected in different well environments (with packers or liners, or in the presence of casing, grout etc.). The ADTS Toolbox permits to automatically estimate the thermal conductivities of the sediments as well as groundwater fluxes all along the heated FO cable. To be usable by the greatest number of users, it includes the automated data interpretation, the evaluation of the quality of estimates, the estimation of uncertainties, and the result visualization. This new tool provides a reliable and easy-to-use approach for characterizing subsurface heterogeneities through the characterization of the variability of both thermal properties and hydraulic conditions at high resolution.

Acknowledgments

Data Availability Statement

The ADTS Toolbox, the associated user guide and the example of application (data and codes) are available and in free access through the following link at database of the H+ French National Network for Hydrogeological sites: http://hplus.ore.fr/en/simon-et-bour-2021-groundwater-data

Authors' Note

The authors do not have any conflicts of interest or financial disclosures to report.

References

Anderson, M.P. 2005. Heat as a ground water tracer. *Ground Water* 43, no. 6: 951–968.

Aufleger, M., M. Conrad, M. Goltz, S. Perzlmaier, and P. Porras. 2007. Innovative dam monitoring tools based on distributed temperature measurement. *Jordan Journal of Civil Engineering* 1: 29–37.

Bakker, M., R. Calje, F. Schaars, K.-J. van der Made, and S. de Haas. 2015. An active heat tracer experiment to determine groundwater velocities using fiber optic cables installed with direct push equipment. *Water Resources Research* 51, no. 4: 2760–2772.

Bakx, W., P. Doornenbal, R.J. Van Weesep, V.F. Bense, G. Oude Essink, and M.F.P. Bierkens. 2019. Determining the relation between groundwater flow velocities and measured temperature differences using active heating-distributed temperature sensing. *Water* 11, no. 8: 1619.

Banks, E., M. Shanafield, and P. Cook. 2014. Induced temperature gradients to examine groundwater flowpaths in open boreholes. *Ground Water* 52, no. 6: 943–951.

Bense, V.F., T. Read, O. Bour, T. Le Borgne, T. Coleman, S. Krause, A. Chalari, M. Mondanos, F. Ciocca, and J.S. Selker. 2016. Distributed temperature sensing as a downhole tool in hydrogeology. *Water Resources Research* 52, no. 12: 9259–9273.

Carslaw, H.S., and J.C. Jaeger. 1959. *Conduction of Heat in Solids*. Oxford University Press.

Coleman, T.I., B.L. Parker, C.H. Maldaner, and M.J. Mondanos. 2015. Groundwater flow characterization in a fractured bedrock aquifer using active DTS tests in sealed boreholes. *Journal of Hydrology* 528: 449–462.

Des Tombe, B., B. Schilperoort, and M. Bakker. 2020. Estimation of temperature and associated uncertainty from fiber-optic Raman-spectrum distributed temperature sensing. *Sensors* 20, no. 8: 2235.

Des Tombe, B.F., M. Bakker, F. Smits, F. Schaars, and K.-J. van der Made. 2019. Estimation of the variation in specific discharge over large depth using distributed temperature sensing (DTS) measurements of the heat pulse response. *Water Resources Research* 55, no. 1: 811–826.

Diao, N., Q. Li, and Z. Fang. 2004. Heat transfer in ground heat exchangers with groundwater advection. *International Journal of Thermal Sciences* 43, no. 12: 1203–1211.

Domanski, M., D. Quinn, F.D. Day-Lewis, M.A. Briggs, D. Werkema, and J.W. Lane Jr. 2020. DTSGUI: A python program to process and visualize fiber-optic distributed temperature sensing data. *Groundwater* 58, no. 5: 799–804.

Fovet, O., M. Ndom, A. Crave, and A. Pannard. 2020. Influence of dams on river water-quality signatures at event and

seasonal scales: The Sélune River (France) case study. *River Research and Applications* 36: 1267–1278.

Galgaro, A., P. Pasquier, L. Schenato, M. Cultrera, and G. Dalla Santa. 2018. Soil thermal conductivity from early TRT logs using an active hybrid optic fibre system. *Proceedings of the IGSHPA Research Track* 2018: 9.

Ghafoori, Y., A. Vidmar, J. Říha, and A. Kryžanowski. 2020. A review of measurement calibration and interpretation for seepage monitoring by optical fiber distributed temperature sensors. *Sensors* 20, no. 19: 5696.

van de Giesen, N., S.C. Steele-Dunne, J. Jansen, O. Hoes, M.B. Hausner, S. Tyler, and J. Selker. 2012. Double-ended calibration of fiber-optic Raman spectra distributed temperature sensing data. *Sensors* 12, no. 5: 5471–5485.

Hakala, P., S. Vallin, T. Arola, and I. Martinkauppi. 2022. Novel use of the enhanced thermal response test in crystalline bedrock. *Renewable Energy* 182: 467–482.

Hausner, M.B., L. Kryder, J. Klenke, R. Reinke, and S.W. Tyler. 2015. Interpreting variations in groundwater flows from repeated distributed thermal perturbation tests. *Groundwater* 54, no. 4: 559–568.

Klepikova, M., C. Roques, S. Loew, and J. Selker. 2018. Improved characterization of groundwater flow in heterogeneous aquifers using granular polyacrylamide (PAM) gel as temporary grout. *Water Resources Research* 54: 1410–1419.

Kurylyk, B.L., and D.J. Irvine. 2019. Heat: An overlooked tool in the practicing hydrogeologist's toolbox. *Groundwater* 57, no. 4: 517–524.

Kurylyk, B.L., D.J. Irvine, and V.F. Bense. 2019. Theory, tools, and multidisciplinary applications for tracing groundwater fluxes from temperature profiles. *Wiley Interdisciplinary Reviews: Water* 6, no. 1: e1329.

Leaf, A.T., D.J. Hart, and J.M. Bahr. 2012. Active thermal tracer tests for improved hydrostratigraphic characterization. *Groundwater* 50, no. 5: 726–735.

Liu, G., S. Knobbe, and J.J. Butler Jr. 2013. Resolving centimeter-scale flows in aquifers and their hydrostratigraphic controls. *Geophysical Research Letters* 40, no. 6: 1098–1103.

Maldaner, C.H., J.D. Munn, T.I. Coleman, J.W. Molson, and B.L. Parker. 2019. Groundwater flow quantification in fractured rock boreholes using active distributed temperature sensing under natural gradient conditions. *Water Resources Research* 55, no. 4: 3285–3306.

Munn, J.D., C.H. Maldaner, T.I. Coleman, and B.L. Parker. 2020. Measuring fracture flow changes in a bedrock aquifer due to open hole and pumped conditions using active distributed temperature sensing. *Water Resources Research* 56, no. 10: e2020WR027229.

Perzlmaier, S., M. Aufleger, and M. Conrad. 2004. Distributed fiber optic temperature measurements in hydraulic engineering: Prospects of the heat-up method. In *Proceedings of a Workshop on Dam Safety Problems and Solutions, 72nd ICOLD Annual Meeting, Seoul, South Korea. 16–22 May 2004*. Int. Commiss, Large Dams, Paris.

Read, T., V.F. Bense, R. Hochreutener, O. Bour, T. Le Borgne, N. Lavenant, and J.S. Selker. 2015. Thermal-plume fibre optic tracking (T-POT) test for flow velocity measurement in groundwater boreholes. *Geoscientific Instrumentation, Methods and Data Systems* 4, no. 2: 197–202.

Read, T., O. Bour, J.S. Selker, V.F. Bense, T.L. Borgne, R. Hochreutener, and N. Lavenant. 2014. Active-distributed temperature sensing to continuously quantify vertical flow in boreholes. *Water Resources Research* 50, no. 5: 3706–3713.

Sayde, C., C.K. Thomas, J. Wagner, and J. Selker. 2015. High-resolution wind speed measurements using actively heated fiber optics. *Geophysical Research Letters* 42, no. 22: 10064–10073.

Selker, F., and J.S. Selker. 2018. Investigating water movement within and near wells using active point heating and fiber optic distributed temperature sensing. *Sensors* 18, no. 4: 1023.

Selker, J.S., L. Thevenaz, H. Huwald, A. Mallet, W. Luxemburg, N. van de Giesen, M. Stejskal, J. Zeman, M. Westhoff, and M.B. Parlange. 2006. Distributed fiber-optic temperature sensing for hydrologic systems. *Water Resources Research* 42, no. 12: W12202.

Simon, N., O. Bour, N. Lavenant, G. Porel, B. Nauleau, B. Pouladi, L. Longuevergne, and A. Crave. 2021. Numerical and experimental validation of the applicability of active-DTS experiments to estimate thermal conductivity and groundwater flux in porous media. *Water Resources Research* 57, no. 1: e2020WR028078.

Simon, N., O. Bour, N. Lavenant, G. Porel, B. Nauleau, B. Pouladi, and L. Longuevergne. 2020. A comparison of different methods to estimate the effective spatial resolution of FO-DTS measurements achieved during sandbox experiments. *Sensors* 20, no. 2: 570.

Stauffer, F., P. Bayer, P. Blum, N. Molina Giraldo, and W. Kinzelbach. 2013. *Thermal Use of Shallow Groundwater*, 1st ed. Boca Raton, FL: CRC Press.

Su, H., S. Tian, Y. Kang, W. Xie, and J. Chen. 2017. Monitoring water seepage velocity in dikes using distributed optical fiber temperature sensors. *Automation in Construction* 76: 71–84.

Sutton, M., D. Nutter, and R. Couvillion. 2003. A ground resistance for vertical bore heat exchangers with groundwater flow. *Journal of Energy Resources Technology* 125, no. 3: 183–189.

Tyler, S.W., J.S. Selker, M.B. Hausner, C.E. Hatch, T. Torgersen, C.E. Thodal, and S.G. Schladow. 2009. Environmental temperature sensing using Raman spectra DTS fiber-optic methods. *Water Resources Research* 45: W00D23.

del Val, L., J. Carrera, M. Pool, L. Martínez, C. Casanovas, O. Bour, and A. Folch. 2021. Heat dissipation test with fiber-optic distributed temperature sensing to estimate groundwater flux. *Water Resources Research* 57, no. 3: e2020WR027228.

Vélez Márquez, I.M., J. Raymond, D. Blessent, M. Philippe, N. Simon, O. Bour, and L. Lamarche. 2018. Distributed thermal response tests using a heating cable and fiber optic temperature sensing. *Energies* 11, no. 11: 3059.

Voytek, E.B., A. Drenkelfuss, F.D. Day-Lewis, R. Healy, J.W. Lane, and D. Werkema. 2014. 1DTempPro: Analyzing temperature profiles for groundwater/surface-water exchange. *Groundwater* 52, no. 2: 298–302.

Zhang, B., K. Gu, B. Shi, C. Liu, P. Bayer, G. Wei, X. Gong, and L. Yang. 2020. Actively heated fiber optics based thermal response test: A field demonstration. *Renewable and Sustainable Energy Reviews* 134: 110336.

Zubair, S.M., and M.A. Chaudhry. 1996. Temperature solutions due to time-dependent moving-line-heat sources. *Heat and Mass Transfer* 31, no. 3: 185–189.